Received: 31 March 2021 | Revised: 26 May 2021 | Accepted: 6 June 2021

DOI: 10.1002/hipo.23373

RESEARCH ARTICLE

WILEY

Adult-born neurons promote cognitive flexibility by improving memory precision and indexing

Gabriel Berdugo-Vega[1] | Chi-Chieh Lee[1] | Alexander Garthe[1,2] | Gerd Kempermann[1,2] | Federico Calegari[1]

[1]CRTD-Center for Regenerative Therapies Dresden, Technische Universität Dresden, Dresden, Germany

[2]DZNE-German Center for Neurodegenerative Diseases, Dresden, Germany

Correspondence
Federico Calegari, CRTD-Center for Regenerative Therapies Dresden, Technische Universität Dresden, Fetscherstrasse 105, Dresden 01307, Germany.
Email: federico.calegari@tu-dresden.de

Funding information
Deutsche Forschungsgemeinschaft, Grant/Award Number: CA893 17-1; H2020 Marie Skłodowska-Curie Actions, Grant/Award Number: 813851

Abstract

Adult neurogenesis in the hippocampal dentate gyrus (DG) is an extraordinary form of plasticity fundamental for cognitive flexibility. Recent evidence showed that newborn neurons differentially modulate input to the infra- and supra-pyramidal blades of the DG during the processing of spatial and contextual information, respectively. However, how this differential regulation by neurogenesis is translated into different aspects contributing cognitive flexibility is unclear. Here, we increased adult-born neurons by a genetic expansion of neural stem cells and studied their influence during navigational learning. We found that increased neurogenesis improved both memory precision and flexibility. Interestingly, each of these gains was associated with distinct subregional patterns of activity and better separation of memory representations in the DG-CA3 network. Our results highlight the role of adult-born neurons in promoting memory precision and indexing and suggests their anatomical allocation within specific DG-CA3 compartments, together contributing to cognitive flexibility.

KEYWORDS
cognitive flexibility, hippocampal neurogenesis, indexing, memory precision

1 | INTRODUCTION

The hippocampal dentate gyrus(DG)-CA3 network is fundamental for the separation and recollection of episodic memories (Rolls, 2013). In addition, this circuit possesses the exceptional ability to incorporate new DG granule cells over the course of life through a process called adult neurogenesis. Adult neurogenesis has been proposed to promote cognitive flexibility, which is defined as the ability to adapt learning to the presence of changing contingencies (Anacker & Hen, 2017; Garthe et al., 2009). This notion was supported by a number of loss of function studies (Burghardt et al., 2012; Clelland et al., 2009; Dupret et al., 2008; Garthe et al., 2009; Niibori et al., 2012) as well as approaches increasing neurogenesis and resulting in improvements in hippocampal-dependent learning in reversal paradigms of spatial navigation and contextual discrimination (Berdugo-Vega et al., 2020; Epp et al., 2016; Garthe et al., 2016; Kent et al., 2015; McAvoy et al., 2015; Sahay et al., 2011; Wang et al., 2014). Understanding the mechanisms triggering neurogenesis-dependent cognitive improvement is thought to be critical for exploiting this form of plasticity to rescue memory deficits in clinical settings.

Importantly, several complex cognitive processes can independently improve flexible learning and contextual discrimination. Among these, mathematical models proposed a role of adult-born neurons in resolving memory interference (Appleby et al., 2011; Wiskott et al., 2006). In parallel, experimental manipulations provided alternative models to explain how such neurogenesis-dependent resolution of memory interference can be achieved by either increasing the

sparsity of neural representations (McAvoy et al., 2015), their consolidation (Kitamura et al., 2009) or, alternatively, forgetting (Akers et al., 2014). These different aspects of cognitive flexibility were intrinsically difficult to disentangle and the specific role(s) of adult-born neurons in memory precision, separation, or clearance remain elusive.

Furthermore, adult-born neurons were proposed to either act as encoding units or regulators of the activity of the more numerous, mature granule cells (Piatti et al., 2013). Independently from their mode of action, effects of neurogenesis were generally assumed to be homogeneous within the DG. However, recent studies highlighted that adult-born neurons differentially modulate input from the entorhinal cortex into the infra- and supra-pyramidal (IP and SP, respectively) blades of the DG (Luna et al., 2019), further supporting the existence of an intrinsic cellular heterogeneity not only within the DG (Erwin et al., 2020; Mishra & Narayanan, 2020), but also its downstream target CA3 (Hunsaker et al., 2008; Sun et al., 2017; Thompson et al., 2008). Given that medial and lateral entorhinal inputs have been suggested to primarily provide spatial and contextual information, respectively (Hargreaves et al., 2005; Knierim et al., 2014), and in turn that such inputs may preferentially be segregated into the IP and SP blades (Luna et al., 2019), we hypothesized that a differential modulatory effect of adult-born neurons within the two blades of the DG and their downstream circuitry may support different aspects of cognitive flexibility. In turn, such anatomical and functional heterogeneity may help reconcile conflicting studies proposing a role of neurogenesis in memory precision, separation, or alternatively, forgetting.

Here, we sought to dissect the different components of neurogenesis-dependent, cognitive flexibility, and their anatomical allocation. To this end, we exploited a mouse model in which increased neurogenesis was achieved by a Cdk4/cyclinD1-dependent expansion of neural stem and progenitor cells (together NSC; Artegiani et al., 2011) that was shown to rescue hippocampal cognitive deficits during aging (Berdugo-Vega et al., 2020). This approach gave us the unique opportunity to investigate the impact of neurogenesis upon generation of an expanded and age-matched cohort of adult-born neurons, thus, avoiding confounding effects resulting from chronic treatments, such as physical exercise, or irreversible genetic manipulation in which neurons of different ages can simultaneously trigger different behavioral effects. We further combined this genetic manipulation of neural stem cells resulting in increased neurogenesis with engram labeling technologies used as a proxy for the identification of behaviorally-induced neuronal activity (Tonegawa et al., 2015) and assessed memory ensembles in the IP and SP blade and CA3 during the processing of spatial information versus memory interference. Together, our study aimed to dissect different aspects of adult neurogenesis in the refinement of memory precision, separation, and clearance, together promoting cognitive flexibility.

2 | RESULTS

2.1 | Transient expansion of NSC results in the generation of a single, age-matched cohort of newborn neurons in the IP and SP blades

Our group already described a method to increase neurogenesis by a genetic expansion of NSC. This was based on the overexpression of Cdk4/cyclinD1 (4D for brevity) in NSC by means of stereotaxic injection of lentiviral particles in the DG. Achieving the temporal control of NSC expansion, a loxp-flanked 4D cassette was used and injections performed in *nestin*::CreERt2 mice. In essence, while viral injection led to overexpression of 4D and NSC expansion, tamoxifen was administered 3 weeks later to terminate this effect and induce the synchronous switch of the expanded cohort of NSC to increased neurogenesis (Artegiani et al., 2011). Having shown the efficacy of this approach (Berdugo-Vega et al., 2020), and similar strategies resulting from it (Bragado Alonso et al., 2019), we here sought to exploit this tool to generate a single wave of age-matched newborn neurons of 4 weeks of age, a timepoint when they are known to display functional integration and enhanced synaptic plasticity before becoming undistinguishable from mature granule cells (Esposito et al., 2005; Gu et al., 2012; Restivo et al., 2015; Temprana et al., 2015). Hence, neuronal maturation, survival, and integration were assessed in 4D-injected mice (2–3 months old), relative to GFP-injected mice used as negative controls, at different times after tamoxifen administration with specific focus on their distribution in the IP and SP blades of the DG.

First, we took advantage of the design of our viral vectors triggering redistribution of a GFP reporter from the nucleus to the cytoplasm upon Cre recombination in NSC (in both control and 4D) and, following 3 weeks of NSC expansion, assessed the morphology of the newborn neurons at subsequent times after tamoxifen administration (2, 4, and 6 weeks) (Figure 1(a)). This showed a comparable progression in the complexity of dendritic arborization, spine density, and axonal projections to the CA3 in GFP-control and 4D-derived newborn neurons over time (Figures 1(b) and S1(a)). Together with previous reports from our group (Berdugo-Vega et al., 2020; Bragado Alonso et al., 2019), these results validated the physiological differentiation and integration of newborn neurons upon 4D overexpression in NSC. At the same time, these experiments also gave us the opportunity to assess whether the increase in neurogenesis triggered by the expansion of NSC was constant or transient. Comparison of the levels of putative NSC (Sox2+S100β−) and early born neurons identified by a marker transiently expressed after birth (Dcx+) within the pool of virally transduced cells (GFP+; Figure S1(b)) confirmed a doubling in the levels of neurogenesis in 4D-injected mice 2 weeks after tamoxifen relative to controls (fold increase: Sox2+S100β− = 2.15 ± 0.39, $p = .026$; Dcx+ = 1.90 ± 0.32, $p = .021$; Figure 1(c), left). In contrast, both NSC and early born neurons returned to physiological levels 4 weeks post tamoxifen (1.12 ± 0.44, $p = .66$ and 0.89 ± 0.16, $p = .77$ fold in 4D relative to control, respectively; Figure 1(c), right) indicating that the increase in neurogenesis triggered by 4D was transient. Yet, the abundance of total 4D-derived neurons identified by cytoplasmic GFP remained the double in 4D relative to GFP-injected mice at 2 and 4 weeks after tamoxifen (GFPcyt+: 2.71 ± 0.38, $p = .012$ and 2.26 ± 0.66, $p = .033$ fold increase, respectively; Figure 1(c)) suggesting that the expanded wave of age-matched newborn neurons was not compensated by increased cell death. This was confirmed by BrdU birthdating 1 week prior to tamoxifen administration and assessment of adult-born neurons 4 weeks later by the use of a

mature marker (NeuN+). This showed that the wave of an increased cohort of neurons was maintained in 4D animals with a doubling in 4 week old neurons relative to controls (NeuN+BrdU+: 2.53 ± 0.35 fold increase, $p = .003$) that was of comparable magnitude in the IP and SP blades (2.12 ± 0.51, $p = .044$ and 3.28 ± 0.88, $p = .013$ fold increase, respectively) and similar among the two groups of mice (IP vs. SP within GFP and 4D: $p = .53$ and $p = .65$, respectively; Figure 1(d)).

Together, our data showed that a transient expansion of NSC can be used to generate a synchronized neurogenic wave in the IP and SP. Several loss of function studies highlighted the effects of ablating neurogenesis in negatively influencing hippocampal function (Burghardt et al., 2012; Clelland et al., 2009; Dupret et al., 2008; Garthe et al., 2009; Niibori et al., 2012). Our approach gave us the unique opportunity to assess the impact of the converse manipulation upon generation of an expanded and age-matched cohort of 4 week old newborn neurons.

2.2 | Increased neurogenesis promotes spatial navigation and flexible learning by differentially modulating the activity of the IP and SP

We next investigated the effect of this increased wave of 4 week old neurons in mouse cognitive function by using a paradigm of the Morris water maze including a learning phase followed by reversal to assess spatial navigation and resolution of memory interference, respectively (Figure 2(a)). Our group recently showed that, in aged mice, assessment of navigational learning strategies can reveal important aspects of cognition that are not necessarily apparent when

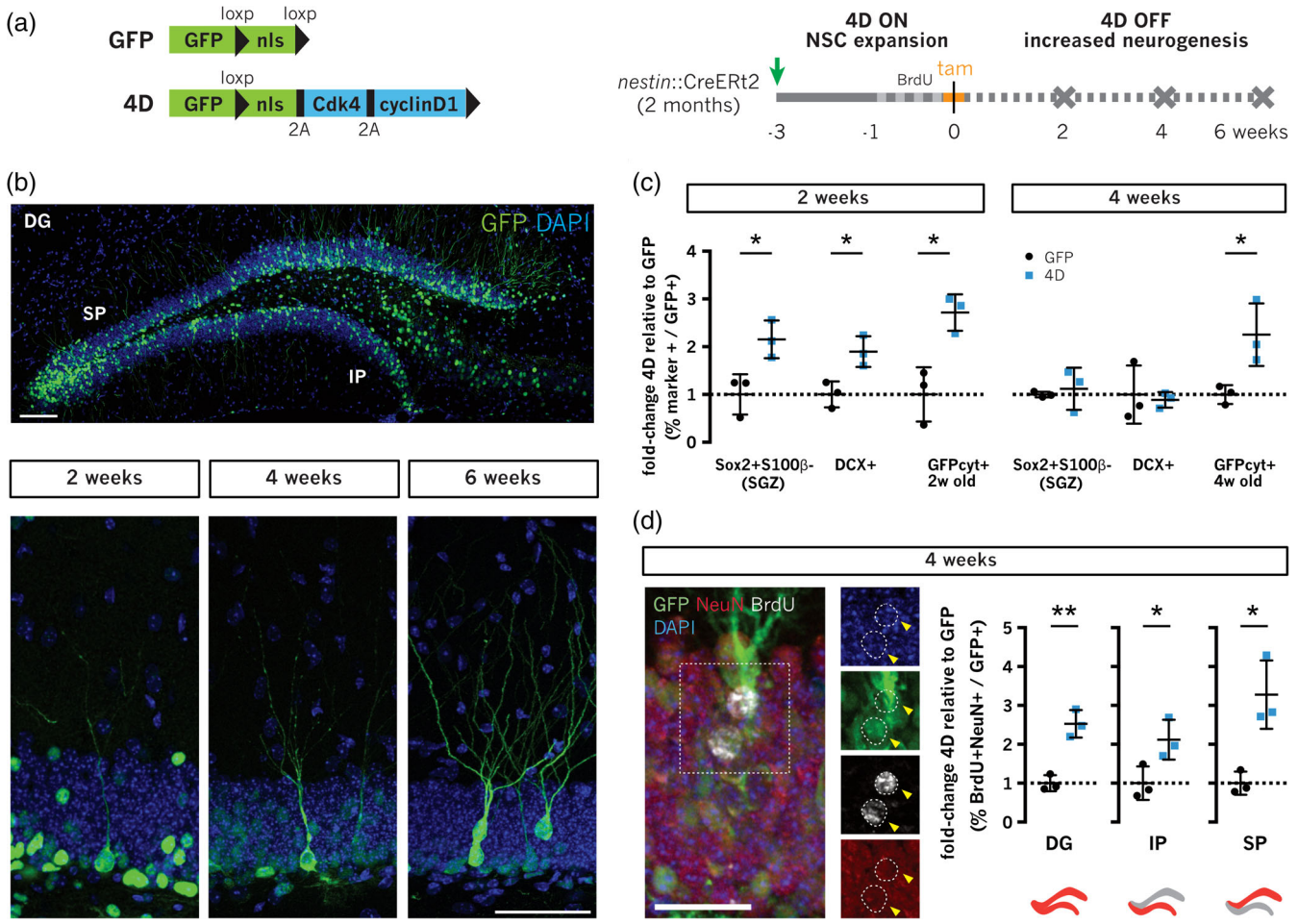

FIGURE 1 NSC expansion generates a single, age-matched cohort of newborn neurons in the IP and SP blades. (a) Scheme depicting the GFP and 4D lentiviral constructs (left) and experimental layout (right) to achieve temporal control of transgenes expression by injection of lentiviruses in the DG of 2–3 month old *nestin*::CreERt2 mice (4D ON) with tamoxifen triggering the recombination of the loxp-flanked functional genes (4D OFF) together with the nuclear localization signal (nls) of GFP. (b–d) Fluorescence pictures and quantifications of cell types identified by immunohistochemistry in the subgranular zone (SGZ) of the DG (c) and IP or SP blades (d) at different times after tamoxifen administration (as indicated). Note the nuclear to cytoplasmic redistribution of GFP in newborn neurons (b; bottom). Examples of cells scored are indicated (d, insets; arrowheads). Scale bars = 100 μm (b) and 50 μm (d). Data represent mean ± *SD* as fold-change within GFP+ infected cells of 4D (blue) relative to GFP (black). $N = 3$; n >500 (SGZ) and >1000 (IP/SP). Unpaired Student's t-test *p <.05; **p <.01. Total cell counts are provided in Supporting Information File S1

assessing behavioral performance alone (Berdugo-Vega et al., 2020). This seemed to also apply in our current study since pathlength analysis of swimming trajectories during both learning and reversal did not highlight any major difference between mice with increased neurogenesis and controls (Figure S2(a)). Hence, we tested GFP and 4D-injected mice 4 weeks after tamoxifen administration to evaluate their evolution in the use of hippocampus-dependent and spatially-precise strategies over time by using an automated machine learning model that assesses swimming trajectories unbiasedly (Overall et al., 2020).

During the learning phase, the increase in the use of hippocampus-dependent strategies at the expense of nonspatial navigation progressed at a similar pace and to a similar degree in both control and 4D mice with increased neurogenesis (yellow vs. greens, N >28; Figure 2(b)). This was different from our recently described effect of increasing neurogenesis in old mice, in which 4D rescued age-dependent deficits by promoting the overall contribution of hippocampal navigation (Berdugo-Vega et al., 2020). However, since young mice already display a very high use of hippocampal navigation, we sought to investigate whether in this context increasing neurogenesis may promote the precision of these learning strategies rather than their overall contribution. Confirming this, the previous unbiased assessment of swimming trajectories revealed a 46% increase in the proportion of the most precise "direct" and "focal" strategies in 4D relative to control mice during learning (logistic regression, odds ratio [OR] = 1.78, p = .002; Figure 2(b), top). This effect was particularly evident in the last day of learning (57% increase, OR = 1.92, p = .004) and among hippocampally scored strategies (58% increase, OR = 2.18, p = .002; Figure 2(b), bottom). Confirming this, on day 3 mice with increased neurogenesis showed overall more direct trajectories (initial trajectory error: 48.7 ± 16.7 vs. 58.7 ± 16.2 cm for 4D and GFP, respectively, p = .020) and shorter pathlengths among hippocampally scored strategies (311.0 ± 167.2 vs. 357.7 ± 165.6 cm for 4D and GFP, respectively, p = .002; Figure S2(b)). Finally, we additionally used the pathlength as a proxy of precision and divided hippocampal strategies in spatially precise or imprecise (pathlengths <1.5 or >1.5 over optimal performance, respectively), finding in mice with increased neurogenesis a 2.3-fold increase in precise strategies relative to controls (OR = 3.02, p = .0001; Figure 2(b), bottom and Figure S2(b)). Together, these results indicated that increasing neurogenesis in young mice with naturally high levels of spatial navigation

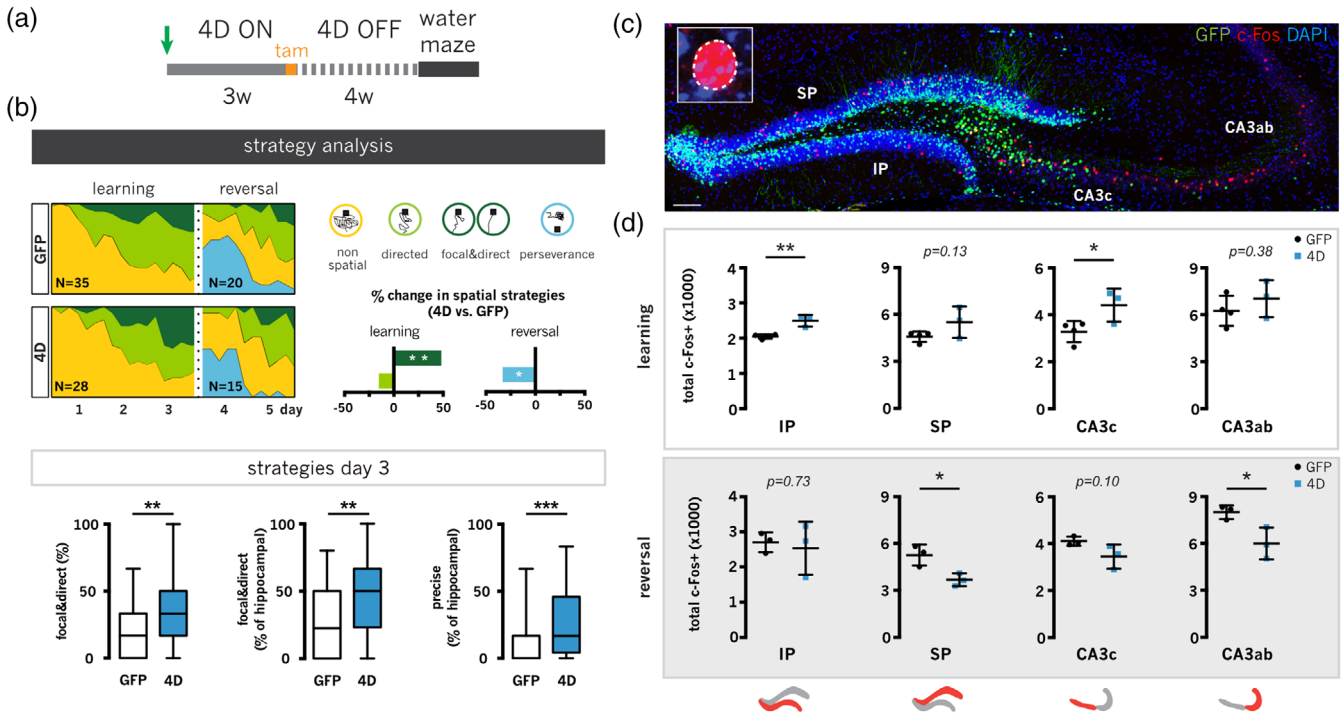

FIGURE 2 Increased neurogenesis promotes spatially precise navigation and flexible learning by differentially modulating the activity of the DG-CA3 circuit. (a–d) Experimental layout (a) and evolution in navigational strategies (b) of GFP and 4D-treated mice subjected to a water maze test after treatment shown in a and sacrificed after the last trial of learning (day 3) or reversal (day 5) for assessment the of c-Fos (c; magnified in inset) in the IP/SP/CA3c/CA3ab compartments (d; as indicated). The same data are also depicted as a comparison between learning versus reversal within groups of GFP or 4D mice in Figure S2(c). Note the increased use of spatially precise strategies during learning and reduced perseverance after reversal (b, top; dark green and blue, respectively) associated with increased c-Fos in the IP-CA3c (d; left) and decrease in the SP-CA3ab (d; right) in 4D (blue) relative to control (black) mice. Precision was defined as a function of pathlength in hippocampally scored strategies (<1.5 optimal performance). Scale bar = 100 μm. Box–Whiskers plots represent the percentage of focal and direct or precise strategies among all (left) or hippocampally scored (middle and right) strategies, as indicated. Data represent mean ± *SD* of total c-Fos + cells. N = 15–35 (b) or 3–4 (d) mice; n >50 (IP/SP) and >90 (CA3). Wald test (b) or unpaired Student's t-test (d) *p <.05; **p <.01. Total cell counts are provided in Supporting Information File 1

did not accelerate the pace in the acquisition of hippocampal learning. Yet, it nonetheless improved the precision of hippocampal strategies once these were acquired.

We then investigated neuronal correlates of spatial memory by performing c-Fos immunohistochemistry of the dorsal hippocampus (Figure 2(c)) with special attention to subregional patterns of activity (Ramírez-Amaya et al., 2005; Snyder et al., 2012). Analysis of mice killed after the last learning trial revealed an increased activity of the DG in 4D-treated mice relative to controls (total estimated c-Fos + per hemisphere: 8034 ± 1102 vs. 6556 ± 359, respectively, $p = .049$; Supporting Information File 1). Further, the number of active granule cells in the IP blade was significantly increased by 22% (2496 ± 167 vs. 2046 ± 62 for 4D and GFP, respectively, $p = .004$) while values in the SP were not significantly changed ($p = .13$; Figure 2 (d), top). Additionally, quantifications in the CA3 area showed an increase by 35% of active cells in its proximal CA3c segment in 4D relative to controls (4411 ± 702 vs. 3279 ± 451, respectively, $p = .047$), with no difference in its distal CA3ab segment (7031 ± 1188 vs. 6251 ± 959, respectively, $p = .38$; Figure 2(d), top). Our observations were consistent not only with the reported role of newborn neurons in increasing neuronal activity within the IP blade of the DG during spatial navigation (Luna et al., 2019), but also with the preferential connection between the IP and the CA3c (Witter, 2007) as a region involved in the processing of spatial information (Hunsaker et al., 2008; Lee et al., 2015). Together, these findings suggested that increased levels of neurogenesis trigger the recruitment of a larger neuronal ensemble in the IP-CA3c circuit in turn improving navigation and memory precision.

To further address the effect of increased neurogenesis in the resolution of memory interference, mice ($N = 15–20$) were additionally trained for 2 days upon reversal of the platform's position to the opposite quadrant of the pool. Analysis of the swimming trajectories showed the appearance of perseverance in both groups and reacquisition of hippocampal-directed strategies thereafter (Figure 2(b)). Remarkably, and indicative of improved flexible learning (Garthe et al., 2009), the contribution of perseverance (blue) to navigational strategies was significantly reduced by 30% in mice with increased neurogenesis (OR = 0.62, $p = .032$; Figure 2(b), top). In turn, this showed that 4D mice were not only more spatially precise during learning, but also able to adapt more flexibly to a changing contingency after reversal.

We next performed a similar assessment of c-Fos in mice after the last trial of reversal. Here, 4D-treated mice showed a general decrease in the activity of the DG (c-Fos+: 6293 ± 876 vs. 7884 ± 727, for 4D and GFP, respectively, $p = .072$; Supporting Information File 1), with a 30% reduction in the number of activated cells in the SP blade (3679 ± 406 vs. 5255 ± 671 in 4D and GFP, respectively, $p = .025$) but no significant changes in the IP blade ($p = .73$; Figure 2 (d), bottom). In addition, quantifications in the CA3 showed an average 20% reduction in activity in 4D brains relative to controls that only reached significance in the distal CA3ab subregion (CA3c: 3446 ± 512 vs. 4106 ± 193, respectively $p = .10$; CA3ab: 5996 ± 1015 vs. 8002 ± 439, respectively, $p = .035$; Figure 2(d), bottom). Together with our previous assessment of neuronal ensembles after learning, these results after reversal were consistent with the role of newborn neurons in decreasing neuronal activity in the SP blade of the DG during the processing of novel contextual information (Luna et al., 2019). In turn, our observed effects in the CA3ab can also be explained by its preferential connectivity with the SP blade (Witter, 2007). In essence, while our previous analysis during learning revealed a link between increased neurogenesis, navigational precision, and the recruiting of larger ensembles in the IP-CA3c circuit, our data upon reversal additionally link increased neurogenesis to flexible learning and, conversely, the recruitment of smaller ensembles in the SP-CA3ab.

These experiments also gave us the opportunity to reanalyze the same c-Fos quantifications but this time considering the intragroup analysis within GFP or 4D mice after learning and reversal. Within the two groups of GFP mice, comparison of c-Fos before and after reversal revealed a general increase in the overall activity of the DG due to elevated counts in the IP blade ($p = .006$) and accompanied by a similar trend in the SP ($p = .13$; Figure S2(c), left). Notably, in control mice a comparable increase in c-Fos was also found in the entire CA3 area (CA3c, $p = .033$; CA3ab, $p = .034$; Figure S2(c), left). Conversely, intragroup comparisons of 4D mice showed that their response to reversal resulted in a general reduction in DG activity through a specific decrease in the SP blade ($p = .043$; Figure S2(c), middle), but not the CA3. Additionally, the activity of the IP-CA3c and SP-CA3ab microcircuits were positively correlated in both groups during learning and reversal, respectively (Figure S2(c), right).

Consistent with a differential modulation of entorhinal input by newborn neurons (Luna et al., 2019), our results showed that increased neurogenesis elevated the activity of the IP-CA3c circuit and that this was associated with the use of more spatially precise strategies during learning indicative of higher memory precision. Additionally, we found that changes in flexible learning were associated with a differential response to the introduction of reversal, with control mice increasing DG-CA3 activity while 4D mice decreased it. Notably, and consistent with a previous report (Stone et al., 2011), none of these changes directly involved the newborn neurons themselves (identified as GFPcyt+ cells) since these where never found to be part of any c-Fos+ ensemble (data not shown) supporting the notion that newborn neurons are strong regulators of local activity (Ikrar et al., 2013; Luna et al., 2019). In addition, we found that behavioral improvements were specifically triggered by 4 week old neurons since no difference in behavior was observed 6 weeks after tamoxifen administration between 4D and control animals (Figure S2(d)).

Knowing that neurogenesis-mediated sparsity was suggested to reduce memory interference (Anacker & Hen, 2017; McAvoy et al., 2015), we next investigated whether animals with increased neurogenesis created new and more separated memory representations in the SP-CA3 circuit after reversal.

2.3 | Cognitive flexibility without forgetting is associated with a better separation of memory indexes in the SP-CA3ab circuit

To directly assess whether neurogenesis-dependent downregulation of SP activity alone decreased the overlap of memory representations,

we sought to identify the ensemble of neurons representing the first learning experience and compare it with that formed after reversal by the use of engram-labeling technology (Reijmers et al., 2007).

GFP and 4D-treated mice were maintained in doxycycline (dox) diet and additionally injected prior to tamoxifen administration with AAV9 viruses encoding *c-Fos*::tTa and *TRE*::mCherry (Figure 3(a)). Mice

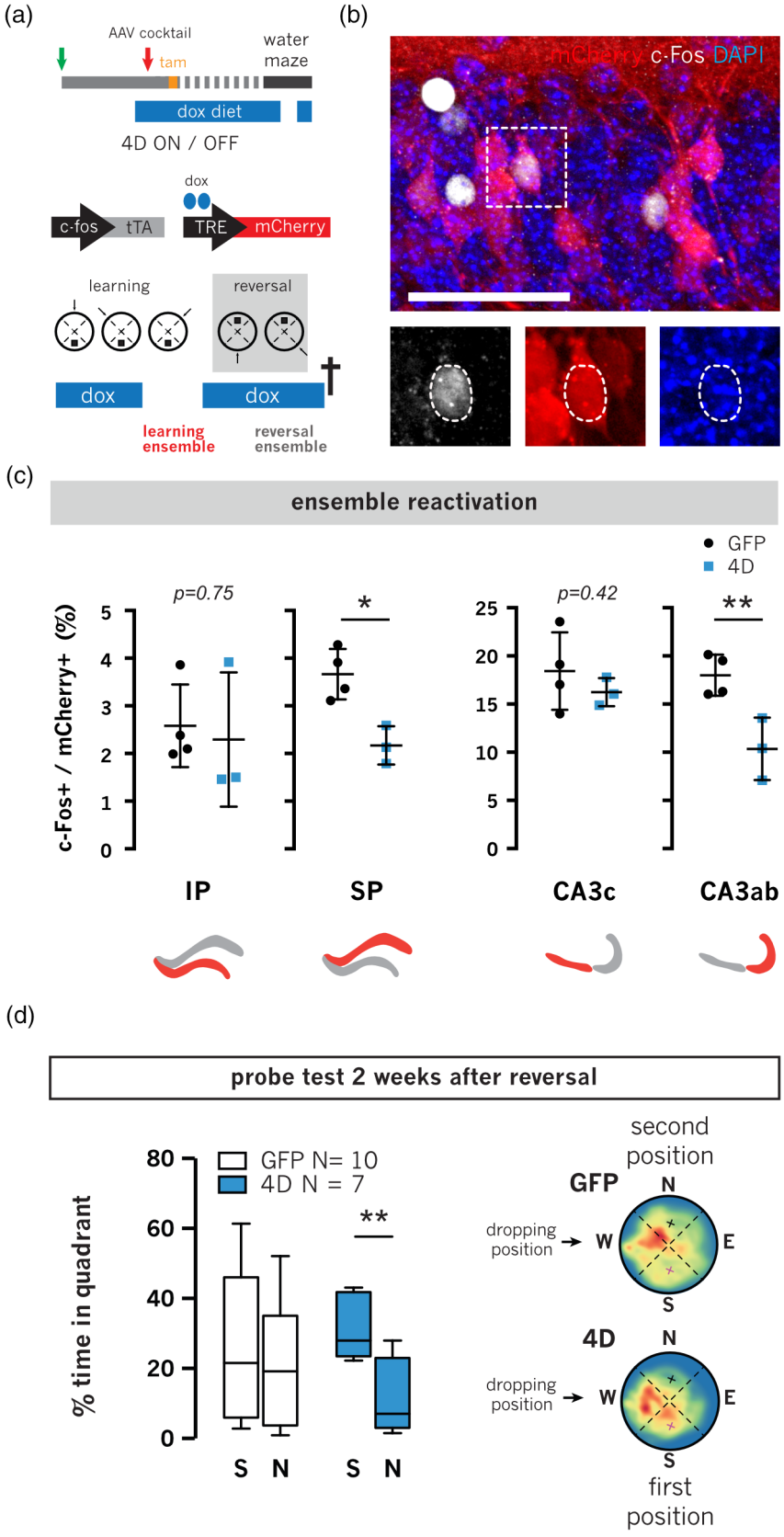

FIGURE 3 Increased neurogenesis facilitates the separation of memory indexes in the SP-CA3ab circuit (a–c) experimental layout (a), fluorescence pictures of ensemble-labeling (b) and quantifications (c) combining the use of AAV9 viruses encoding for *c-Fos*::tTa and *TRE*::mCherry with dox treatment for the labeling of remote (mCherry+) and recent (c-Fos+) memory representations. Note the reduction in reactivation rate specifically within the SP and CA3ab areas (c). These data are also depicted relative to chance reactivation in Figure S3(b). (d) Box–Whisker plots (left) and heatmaps (right) displaying quadrant preference of mice tested 2 weeks after treatment shown in a. Note the increased preference of mice with increased neurogenesis for the first position of the platform. Scale bar = 100 μm. Data represent mean ± *SD* as the proportion of reactivated cells within the mCherry+ population in different DG-CA3 compartments (c) or Box–Whisker plots (d) of 4D (blue) and controls (black). $N = 3–4$ (c) and 7–10 (d); n >400 (IP/SP) and >100 (CA3). Unpaired Student's t-test $^{*}p < .05$; $^{**}p < .01$. Total cell counts are provided in Supporting Information File 1

were trained in the water maze and dox removed from the diet 24 h before the last day of the learning phase to allow the activity-dependent labeling of the memory ensemble representing the first experience. Immediately after the last trial of learning, dox was reintroduced and mice subjected to two additional days of reversal and killed after the last trial (Figure 3(a)). The reactivation rate was finally assessed as defined by the proportion of cells belonging to the remote memory ensemble (mCherry+) that were also recruited by the recent memory (c-Fos+ revealed by immunohistochemistry; Figures 3(b) and S3(a)). This showed that reactivation in the DG of 4D mice was ca. 30% lower than in controls (2.25 ± 0.42 vs. 3.30 ± 0.56%, respectively, $p = .043$; Supporting Information File 1). Interestingly, we found a ca. 40% reduction in reactivation in both the SP blade (2.17 ± 0.40 vs. 3.66 ± 0.53, $p = .010$; Figure 3(c)) and in the CA3ab of 4D animals (10.35 ± 3.23 vs. 18.00 ± 2.13%, $p = .005$) while no differences in reactivation could be observed in neither the IP nor CA3c ($p = .75$ and .42, respectively; Figure 3(c)). Since these values may potentially also be influenced by different AAV infectivity rates among granule cells (DAPI) or varying efficiency of the reporter induction (mCherry), we sought to assess whether these reactivation rates in GFP and 4D mice were significantly different from those expected from chance alone.

To this aim, we calculated the probability of chance co-labeling ($P_{mCherry+}$ $^{*}P_{c\text{-}Fos+}$ relative to DAPI+) in individual mice and found that while total reactivation in the SP blade was significantly above chance in control (0.30 ± 0.06 vs. 0.17 ± 0.09%, $p = .006$) it was less so and not significantly in 4D mice (0.20 ± 0.05 vs. 0.12 ± 0.01%, $p = .085$; Figure S3(b)). This effect was also mirrored in the CA3ab with chance levels of reactivation in control (4.06 ± 0.27 vs. 5.66 ± 2.69%, $p = .28$) and, remarkably, even below chance in 4D mice (1.29 ± 0.73 vs. 1.63 ± 0.69, $p = .040$; Figure S3(b)). In turn, this is consistent with the notion that neurogenesis promotes the separation of memory indexes by increasing the sparsity of neural representations and thereby reduce the mere statistical probability that any given neuron is being re-activated twice in consecutive experiences (McAvoy et al., 2015). Hence, we expected that a strong positive correlation would emerge when comparing c-Fos levels and reactivation rates within the SP blade.

However, no obvious correlation could be found in neither control, 4D mice or pooling them together ($r = .45$, $p = .30$; Figure S3(c)) and even the single mouse among controls showing the lowest level of c-Fos after reversal still displayed the highest level of SP reactivation (ca. 25% lower and 16% higher than the group mean, respectively; Figure S3(c), red dot). Intrigued by this unexpected lack in correlation within the SP blade, we next calculated the density of c-Fos+ ($P_{c\text{-}Fos}$) cells that would be required to reduce total reactivation of GFP mice to their chance levels, as it was the case for 4D-treated animals, and resulting in a mathematically extrapolated reduction by 42.3 ± 19.5%, (i.e., from 1.71 ± 0.34 to 0.98 ± 0.09%). Surprisingly, this value was greater ($p = .043$) than the measured 13.9 ± 5.06% reduction in the density of c-Fos+ cells in the SP of 4D mice relative to controls (i.e., from 1.71 ± 0.34 to 1.47 ± 0.09%). In other words, the extrapolated reduction in c-Fos necessary for control mice to reach chance levels was significantly greater than the reduction

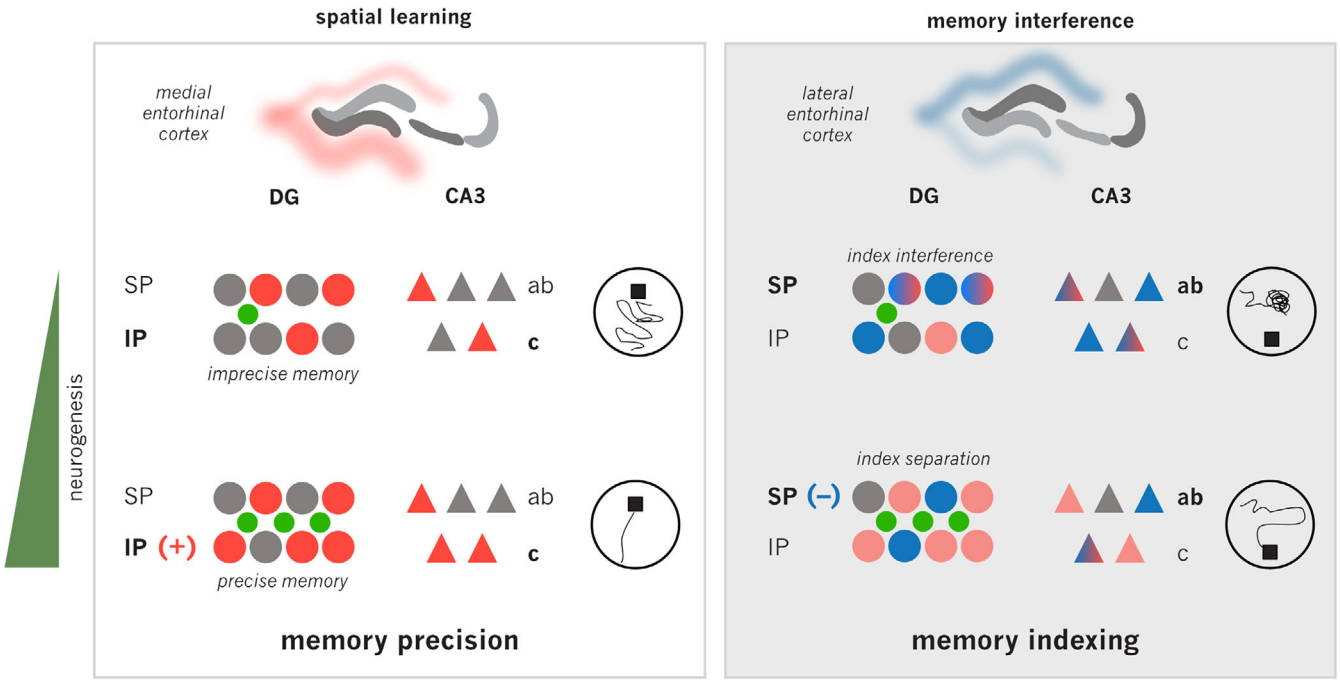

FIGURE 4 Model of input integration and DG blades regulation by adult-born neurons in cognitive flexibility. Together with a number of previous studies (see text), our study proposes a new model thereby input from the medial versus lateral entorhinal cortex and carrying spatial versus novel contextual information is differentially modulated by adult-born neurons of the IP versus SP blades of the DG, which in turn modify activity patterns in the downstream CA3c versus CA3ab and, finally, is translated into gains in memory precision versus indexing, respectively

observed in 4D mice. In turn, this suggested that neurogenesis can decrease reactivation rate in the SP beyond a mere reduction in the statistical probability of co-activation due to sparsity alone.

Finally, since neurogenesis has also been proposed to resolve interference through the forgetting of conflicting old memories (Epp et al., 2016), we investigated if the increased flexibility of 4D mice was also accompanied by attenuation of the memory of the first, learnt position of the platform by a probe trial 2 weeks after reversal. While GFP mice showed no preference for neither the first nor the second platform position (time in quadrants: 26.26 ± 21.73 vs. 20.13 ± 17.41%, respectively, $p = .49$), mice with increased neurogenesis preserved a clear preference for the first platform position (31.64 ± 8.94 vs. 12.18 ± 10.28%, $p = .003$; Figure 3(d)). This indicated that the reduction of interference in animals with increased neurogenesis was not associated with forgetting of the first experience.

Altogether, our data showed that increasing neurogenesis allowed mice not only to learn more precisely, but also to better resolve interference while at the same time retaining past memories. In addition, we found that these cognitive gains were associated with the recruitment of larger ensembles in the IP-CA3c and a better separation of memory indexes in the SP-CA3ab, respectively. In turn, our study suggests that specific functions underlying cognitive flexibility such as memory precision and indexing are anatomically allocated to distinct DG-CA3 circuits that are differentially modulated by adult neurogenesis (as modeled in Figure 4).

3 | DISCUSSION

Here we found that a cell intrinsic, genetic expansion of NSC increasing hippocampal neurogenesis differentially modulated DG-CA3 activity during learning and improved cognitive flexibility. Importantly, the use of a previously characterized 4D model (Berdugo-Vega et al., 2020; Bragado Alonso et al., 2019) provided us with an unprecedented level of specificity for gain-of-function studies by the generation of a single cohort of age-matched neurons. This led us to address specific roles of 4 week old neurons in promoting different aspects of cognitive flexibility. By looking at different phases of learning versus reversal during navigation we further identified the activity patterns in the DG-CA3 circuit that correlated with improvements in memory precision and indexing.

Specifically, while neurogenesis did not have major effects in the progression from nonhippocampal to spatial navigation, it however promoted more spatially precise trajectories once hippocampal navigation was acquired. This behavioral gain was associated with an increased activity of the IP blade and CA3c that did not directly involve the newborn neurons themselves. Considering that pyramidal CA3c and granule DG neurons were suggested to be more spatially tuned than pyramidal CA3ab and newborn neurons, respectively (Danielson et al., 2016; Lee et al., 2015), our study suggests that the effect of neurogenesis in recruiting a larger neuronal ensemble within the IP-CA3c provides a better and more detailed spatial representation thereby improving memory precision (Figure 4, left).

Moreover, and consistent with previous reports (Burghardt et al., 2012; Garthe et al., 2009, 2016), upon reversal animals with increased neurogenesis displayed higher levels of flexibility. However, the nature of this flexibility and its significance at the level of memory representations remained elusive. In fact, to the best of our knowledge only two previous studies investigated the effects of neurogenesis in the separation of memory engrams during contextual discrimination (Denny et al., 2014; McAvoy et al., 2016). Yet, without discriminating local effects within DG-CA3 subregions and without separating behavioral effects in terms of memory precision versus interference. We showed that neurogenesis-dependent sparsity in the SP blade after reversal reduced the overlap in SP-CA3ab memory representations, which is fundamental to achieve a better resolution of memory interference. Supporting the notion that newborn neurons act as novelty detectors (Denny et al., 2012), neurogenesis may facilitate the allocation of novel experiences to new or more distinct neuronal ensembles in the DG, CA3, or both (Denny et al., 2014; McAvoy et al., 2015; Niibori et al., 2012). Since the reduction in SP-CA3ab activity in our study was not mediated by feedforward inhibition as indicated by the similar levels of active, c-Fos+, parvalbumin+ interneurons in the CA3 (not shown), we infer that the reduced reactivation rate of the CA3ab is likely a direct result of changes in the SP blade that together dictate the recruitment of non-overlapping SP-CA3ab memory ensembles. Reminiscent of the index theory (Teyler & DiScenna, 1986), and consistent with the proposed role of adult neurogenesis in increasing memory capacity (Miller & Sahay, 2019), our study suggests a role of newborn neurons in promoting indexing within the SP (Figure 4, right).

Finally, improvements in memory precision and indexing after increased neurogenesis did not occur at the cost of forgetting. This is fundamental and an intrinsic component of cognitive flexibility as the ability to acquire new memories without forgetting past ones. Intriguingly, control animals reacted to the introduction of novelty by promoting DG-CA3 activity, likely increasing the chance of interference between newly and previously formed memories. In contrast, a reduced activity in conditions of increased neurogenesis may reduce such interference and as a result help forming new, while also preserving past, memories. It was surprising to observe that such effect of neurogenesis appeared to be even more potent than what deduced from a reduced statistical probability due to sparsity alone. This is even more remarkable when considering that reversal did not decreased the overall activity of the CA3ab in 4D animals, but still this area showed levels of reactivation lower than what expected by chance. These improvements may be highly relevant in the context of neurodegenerative disorders causing memory interference, as recently demonstrated in models of Alzheimer disease (Poll et al., 2020).

Adult neurogenesis has long been proposed to promote flexibility in learning but the cognitive processes underlying such flexibility remained elusive. Our study dissects the anatomical and functional contribution of newborn neurons in promoting the formation of more precise and better indexed memories in the DG-CA3 circuit. It also provides insight into how plasticity modulates brain function to cope with an ever-changing environment, which is

relevant for the understanding and treatment of memory disorders ranging from posttraumatic stress to injury and from aging to neurodegeneration.

4 | MATERIALS AND METHODS

4.1 | Viral preparations

Lentiviruses were produced by polyethyleneimine co-transfection of 293T cells with the respective transfer vectors encoding for GFP or 4D, HIV-1 gag/pol and VSV-G as previously described (Artegiani et al., 2011, 2012; Berdugo-Vega et al., 2020). 4D viruses encoded for the three transgenes (GFPnls/Cdk4/cyclinD1) linked by 2A peptides and with LoxP sites allowing the recombination of the 4D cassette together with the nls of GFP. Similar, floxed-nls-GFP vectors were used for control viral particles. One day after transfection, cells were switched to serum free medium and 1 day later the filtered supernatants were centrifuged at 25,500 rpm for 4 h. The viral particles were suspended in 40 μl of PBS per 10 cm petri dish and further concentrated using centrifugal filters (Amicon) yielding ca. 40 μl of virus suspension per construct with a titer of 10^8–10^9 IU/ml as assessed on HEK cells. A video of this protocol is available (Artegiani et al., 2012). AAV9 viruses for the reactivation experiment were produced by $CaPO_4$ co-transfection of AAV293 cells (Stratagene, La Jolla) with the pAAV-cFos::tTA or pAAV-TRE::mCherry (gifts from William Widsen, Addgene plasmids #66794 and #66795), pHelper, and pCR9. Cells were switched to fresh medium 8 h later and collected 2 days thereafter for freeze/thaw lysis. AAV particles were purified from the cell lysate by iodixanol gradient centrifugation (63,000 rpm for 2 h) and then washed in PBS and concentrated (Amicon filters) in successive centrifugation steps (4000*g* for 1 min). Viral titer was assessed by qPCR (10^{10} genome copies/ml).

4.2 | Animal treatments

Mice were kept in standard cages with a 12 h light cycle and water and food ad libitum. In all experiments, female *nestin*::CreRTt2 (Imayoshi et al., 2006) mice in a C57BL/6j genetic background were used. Briefly, isofluorane-anesthetized mice were stereotaxically injected with 1 μl per hemisphere of HIV viral suspension in the DG hilus as previously reported (Artegiani et al., 2012) using a nanoliter-2000 injector (World Precision Instruments) and a stereotaxic frame Model 900 (Kopf Instruments) at ±1.6 mm mediolateral, −1.9 anteriorposterior, and −1.9 mm dorsoventral from bregma with a constant flow of 200 nl/min. For reactivation experiments, animals were switched to doxycycline diet (dox, 40 ppm, ENVIGO) 4 days before viral injections. AAV9 mixtures were obtained by dilution of *c-Fos*::tTA and *TRE*::mCherry viruses in PBS and injected in the DG hilus to find the optimal infectivity for ensemble labeling (reached at 1:20 dilution). Dox diet was replaced by regular diet 24 h before the last day of learning and reintroduced after the last trial. Recombination of the 4D cassette and nls of GFP was achieved by oral administration of tamoxifen (Sigma) dissolved in corn oil (1:10) at 500 mg/kg body weight once a day for 3 nonconsecutive days. BrdU (Sigma) diluted in PBS was intraperitoneally injected at 50 mg/kg concentration. Animals were either subjected to the water maze and/or anesthetized with pentobarbital and transcardially perfused with saline followed by 4% paraformaldehyde (PFA) fixation in phosphate buffer. Perfusions for c-Fos quantifications were performed 90 min after the last trial of navigation.

4.3 | Cellular quantifications

Brains were postfixed overnight in 4% PFA at 4°C and cut in coronal 40 μm thick vibratome sections serially collected along the rostro-caudal axis of the hippocampus and stored at −20°C in cryoprotectant solution (25% ethylene glycol and 25% glycerol in PBS). Immunohistochemistry was performed stereologically in 1 every 6 sections (i.e., 10–12 sections analyzed per brain) after blocking and permeabilization with 10% donkey serum in 0.3% Triton X-100 in PBS for 1.5 h at room temperature. Primary and secondary antibodies (Table S1) were incubated in 3% donkey serum in 0.3% Triton X-100 in PBS overnight at 4°C. For BrdU detection sections were exposed to HCl 2M for 25 min at 37°C. DAPI was used to counterstain nuclei. Pictures were acquired using an automated Zeiss ApoTome or confocal (LSM 780) microscopes (Carl Zeiss) and maximal intensity projections of three optical sections (10 μm thick in total) taken and quantified using Photoshop CS5 (Adobe) and Affinity Photo. In all cases, GFP immunohistochemistry was performed to assess infectivity, which was confirmed in the vast majority (>90%) of the cases. Quantifications were performed on one series of DG sections per animal considering the subgranular zone (for NSC) or the whole thickness of the granular cell layer (for immature and mature neurons) of both the dorsal and ventral hippocampus. Neuronal activity was quantified in the IP and SP blades of the DG in the dorsal hippocampus (from −1.3 to −2.3 from Bregma) and reported as total number of c-Fos+ cells or density relative to DAPI ($P_{\text{c-Fos}}$, P_{mCherry}), extrapolated for the whole anatomical region being considered. Reactivation rate and total reactivation refer to the proportion of c-Fos+mCherry+ within the mCherry+ labeled cells and over the estimated number of DAPI, respectively, whereas chance reactivation was calculated as the intersection of individual probabilities for a given DAPI cell to be c-Fos+ and mCherry+ (% $P_{\text{c-Fos}} * P_{\text{mCherry}}$). Areas were measured using Fiji 1.45b (ImageJ) and morphometric analyses performed on confocal reconstructions through the entire section to include most processes that were later traced and visualized using Fiji (ImageJ).

4.4 | Assessment of navigation

Behavioral experiments were performed in a Morris Water Maze located in a noise-isolated room with strong illumination (300 lux) and consisting of a learning (3 days) and reversal (2 days) phases, six trials

per day as previously described (Garthe et al., 2009). Briefly, after acclimatization to the testing room (15 min) sessions were tracked using the Ethovision system (Noldus). At the end of each trial mice were guided to the platform and then placed in an individual drying cage. In the reversal phase, the platform was relocated at 180 degrees. Probe tests consisted of a single trial for 1 min without platform. Navigational strategies were assessed by unbiased and automatic analysis of the swimming trajectories (Rtrack, Overall et al., 2020) and assigning each trial one predominant strategy among nonhippocampal, hippocampal (directed, focal, and direct) or perseverance. Hippocampal strategies were further divided into precise and imprecise as a function of pathlengths (within or above a 1.5 threshold from optimal performance, respectively) and the initial trajectory error (the remaining distance left after a mouse has completed a path equal to the minimal trajectory) calculated using the Rtrack software. Quadrant occupancy was calculated using Ethovision.

4.5 | Statistics

Quantification of cell types and morphometric analyses were performed on independent biological replicates (see respective figure legends for N = mice and n = cells/dendritic segments/spines/trials counted per mouse) and depicted as means ± *SD*s or Box–Whisker plots with significance being assessed by two-tailed, unpaired (different animals) or paired (total vs. chance reactivation) Student's *t*-test, or Pearson's correlation. Behavioral analyses were performed on 15–35 mice per group (as indicated in figure legends) and data depicted as area charts (navigational strategies) or Box–Whisker plots (pathlengths and probe tests). Statistical significance was accordingly calculated by Wald test of odds ratios assessed by logistic regression (navigational strategies), Mann–Whitney test (pathlengths of hippocampal strategies), or two-tailed unpaired Student's *t*-test (quadrant occupancy and performance).

ACKNOWLEDGMENTS

The authors thank Simon Hertlein for technical assistance, Dr. Tomás Ryan for support with engram labeling experiments and Dr. Antoine Besnard for help in the interpretation of the neuronal activity data. This work was supported by the CRTD, TU Dresden, DFG CA893 17-1, a DIGS-BB fellowship awarded to Gabriel Berdugo-Vega and EU-H2020 Marie Skłodowska-Curie grant (813851) to Chi-Chieh Lee. Open Access funding enabled and organized by Projekt DEAL.

CONFLICT OF INTEREST

The authors declare no conflict of interest in this study.

AUTHOR CONTRIBUTIONS

Gabriel Berdugo-Vega and Federico Calegari conceived the project, analyzed the data and wrote the manuscript. Alexander Garthe and Gerd Kempermann established analyses of navigational strategies and supported their interpretation. Gabriel Berdugo-Vega performed all experiments supported by Chi-Chieh Lee. All authors contributed and approved the final manuscript. Animal experiments were approved by local authorities (TVV 39/2015 and TVV 56/2018).

DATA AVAILABILITY STATEMENT

Data is available from authors upon request.

ORCID

Federico Calegari https://orcid.org/0000-0002-3703-2802

REFERENCES

Akers, K. G., Martinez-Canabal, A., Restivo, L., Yiu, A. P., Cristofaro, A. D., Hsiang, H.-L., Wheeler, A. L., Guskjolen, A., Niibori, Y., Shoji, H., et al. (2014). Hippocampal neurogenesis regulates forgetting during adulthood and infancy. *Science*, *344*, 598–602.

Anacker, C., & Hen, R. (2017). Adult hippocampal neurogenesis and cognitive flexibility — Linking memory and mood. *Nature Reviews. Neuroscience*, *18*, 335–346.

Appleby, P. A., Kempermann, G., & Wiskott, L. (2011). The role of additive neurogenesis and synaptic plasticity in a hippocampal memory model with grid-cell like input. *PLoS Computational Biology*, *7*, e1001063.

Artegiani, B., Lange, C., & Calegari, F. (2012). Expansion of embryonic and adult neural stem cells by in utero electroporation or viral stereotaxic injection. *Journal of Visualized Experiments*, (68), 4093.

Artegiani, B., Lindemann, D., & Calegari, F. (2011). Overexpression of cdk4 and cyclinD1 triggers greater expansion of neural stem cells in the adult mouse brain. *The Journal of Experimental Medicine*, *208*, 937–948.

Berdugo-Vega, G., Arias-Gil, G., López-Fernández, A., Artegiani, B., Wasielewska, J. M., Lee, C.-C., Lippert, M. T., Kempermann, G., Takagaki, K., & Calegari, F. (2020). Increasing neurogenesis refines hippocampal activity rejuvenating navigational learning strategies and contextual memory throughout life. *Nature Communications*, *11*, 1–12.

Bragado Alonso, S., Reinert, J. K., Marichal, N., Massalini, S., Berninger, B., Kuner, T., & Calegari, F. (2019). An increase in neural stem cells and olfactory bulb adult neurogenesis improves discrimination of highly similar odorants. *The EMBO Journal*, *38*(6), e98791.

Burghardt, N. S., Park, E. H., Hen, R., & Fenton, A. A. (2012). Adult-born hippocampal neurons promote cognitive flexibility in mice. *Hippocampus*, *22*, 1795–1808.

Clelland, C. D., Choi, M., Romberg, C., Clemenson, G. D., Fragniere, A., Tyers, P., Jessberger, S., Saksida, L. M., Barker, R. A., Gage, F. H., et al. (2009). A functional role for adult hippocampal neurogenesis in spatial pattern separation. *Science*, *325*, 210–213.

Danielson, N. B., Kaifosh, P., Zaremba, J. D., Lovett-Barron, M., Tsai, J., Denny, C. A., Balough, E. M., Goldberg, A. R., Drew, L. J., Hen, R., et al. (2016). Distinct contribution of adult-born hippocampal granule cells to context encoding. *Neuron*, *90*, 101–112.

Denny, C. A., Burghardt, N. S., Schachter, D. M., Hen, R., & Drew, M. R. (2012). 4- to 6-week-old adult-born hippocampal neurons influence novelty-evoked exploration and contextual fear conditioning. *Hippocampus*, *22*, 1188–1201.

Denny, C. A., Kheirbek, M. A., Alba, E. L., Tanaka, K. F., Brachman, R. A., Laughman, K. B., Tomm, N. K., Turi, G. F., Losonczy, A., & Hen, R. (2014). Hippocampal memory traces are differentially modulated by experience, time, and adult neurogenesis. *Neuron*, *83*, 189–201.

Dupret, D., Revest, J.-M., Koehl, M., Ichas, F., Giorgi, F. D., Costet, P., Abrous, D. N., & Piazza, P. V. (2008). Spatial relational memory requires hippocampal adult neurogenesis. *PLoS One*, *3*, e1959.

Epp, J. R., Silva Mera, R., Köhler, S., Josselyn, S. A., & Frankland, P. W. (2016). Neurogenesis-mediated forgetting minimizes proactive interference. *Nature Communications*, *7*, 10838.

Erwin, S. R., Sun, W., Copeland, M., Lindo, S., Spruston, N., & Cembrowski, M. S. (2020). A sparse, spatially biased subtype of mature granule cell dominates recruitment in hippocampal-associated behaviors. *Cell Reports*, *31*, 107551.

Espósito, M. S., Piatti, V. C., Laplagne, D. A., Morgenstern, N. A., Ferrari, C. C., Pitossi, F. J., & Schinder, A. F. (2005). Neuronal differentiation in the adult hippocampus recapitulates embryonic development. *Journal of Neuroscience*, *25*, 10074–10086.

Garthe, A., Behr, J., & Kempermann, G. (2009). Adult-generated hippocampal neurons allow the flexible use of spatially precise learning strategies. *PLoS One*, *4*, e5464.

Garthe, A., Roeder, I., & Kempermann, G. (2016). Mice in an enriched environment learn more flexibly because of adult hippocampal neurogenesis. *Hippocampus*, *26*, 261–271.

Gu, Y., Arruda-Carvalho, M., Wang, J., Janoschka, S. R., Josselyn, S. A., Frankland, P. W., & Ge, S. (2012). Optical controlling reveals time-dependent roles for adult-born dentate granule cells. *Nature Neuroscience*, *15*, 1700–1706.

Hargreaves, E. L., Rao, G., Lee, I., & Knierim, J. J. (2005). Major dissociation between medial and lateral entorhinal input to dorsal hippocampus. *Science*, *308*, 1792–1794.

Hunsaker, M. R., Rosenberg, J. S., & Kesner, R. P. (2008). The role of the dentate gyrus, CA3a,b, and CA3c for detecting spatial and environmental novelty. *Hippocampus*, *18*, 1064–1073.

Ikrar, T., Guo, N., He, K., Besnard, A., Levinson, S., Hill, A., Lee, H.-K., Hen, R., Xu, X., & Sahay, A. (2013). Adult neurogenesis modifies excitability of the dentate gyrus. *Frontiers in Neural Circuits*, *7*(204).

Imayoshi, I., Toshiyuki, O., Daniel, M., Pierre, C., & Ryoichiro, K. (2006). Temporal regulation of Cre recombinase activity in neural stem cells. *Genesis*, *44*, 233–238.

Kent, B. A., Beynon, A. L., Hornsby, A. K. E., Bekinschtein, P., Bussey, T. J., Davies, J. S., & Saksida, L. M. (2015). The orexigenic hormone acylghrelin increases adult hippocampal neurogenesis and enhances pattern separation. *Psychoneuroendocrinology*, *51*, 431–439.

Kitamura, T., Saitoh, Y., Takashima, N., Murayama, A., Niibori, Y., Ageta, H., Sekiguchi, M., Sugiyama, H., & Inokuchi, K. (2009). Adult neurogenesis modulates the hippocampus-dependent period of associative fear memory. *Cell*, *139*, 814–827.

Knierim, J. J., Neunuebel, J. P., & Deshmukh, S. S. (2014). Functional correlates of the lateral and medial entorhinal cortex: Objects, path integration and local–global reference frames. *Philosophical Transactions of the Royal Society B: Biological Sciences*, *369*(1635), 20130369.

Lee, H., Wang, C., Deshmukh, S. S., & Knierim, J. J. (2015). Neural population evidence of functional heterogeneity along the CA3 transverse axis: Pattern completion versus pattern separation. *Neuron*, *87*, 1093–1105.

Luna, V. M., Anacker, C., Burghardt, N. S., Khandaker, H., Andreu, V., Millette, A., Leary, P., Ravenelle, R., Jimenez, J. C., Mastrodonato, A., et al. (2019). Adult-born hippocampal neurons bidirectionally modulate entorhinal inputs into the dentate gyrus. *Science*, *364*, 578–583.

McAvoy, K., Besnard, A., & Sahay, A. (2015). Adult hippocampal neurogenesis and pattern separation in DG: A role for feedback inhibition in modulating sparseness to govern population-based coding. *Frontiers in Systems Neuroscience*, *9*, 120.

McAvoy, K. M., Scobie, K. N., Berger, S., Russo, C., Guo, N., Decharatanachart, P., Vega-Ramirez, H., Miake-Lye, S., Whalen, M., Nelson, M., et al. (2016). Modulating neuronal competition dynamics in the dentate gyrus to rejuvenate aging memory circuits. *Neuron*, *91*, 1356–1373.

Miller, S. M., & Sahay, A. (2019). Functions of adult-born neurons in hippocampal memory interference and indexing. *Nature Neuroscience*, *22* (10), 1565–1575.

Mishra, P., & Narayanan, R. (2020). Heterogeneities in intrinsic excitability and frequency-dependent response properties of granule cells across the blades of the rat dentate gyrus. *Journal of Neurophysiology*, *123*, 755–772.

Niibori, Y., Yu, T.-S., Epp, J. R., Akers, K. G., Josselyn, S. A., & Frankland, P. W. (2012). Suppression of adult neurogenesis impairs population coding of similar contexts in hippocampal CA3 region. *Nature Communications*, *3*, 1253.

Overall, R.W., Zocher, S., Garthe, A., and Kempermann, G. (2020). Rtrack: A software package for reproducible automated water maze analysis. *BioRxiv*, 2020.02.27.967372.

Piatti, V. C., Ewell, L. A., & Leutgeb, J. K. (2013). Neurogenesis in the dentate gyrus: Carrying the message or dictating the tone. *Frontiers in Neuroscience*, *7*, 50.

Poll, S., Mittag, M., Musacchio, F., Justus, L. C., Giovannetti, E. A., Steffen, J., Wagner, J., Zohren, L., Schoch, S., Schmidt, B., et al. (2020). Memory trace interference impairs recall in a mouse model of Alzheimer's disease. *Nature Neuroscience*, *23*, 952–958.

Ramírez-Amaya, V., Vazdarjanova, A., Mikhael, D., Rosi, S., Worley, P. F., & Barnes, C. A. (2005). Spatial exploration-induced arc mRNA and protein expression: Evidence for selective, network-specific reactivation. *The Journal of Neuroscience*, *25*, 1761–1768.

Reijmers, L. G., Perkins, B. L., Matsuo, N., & Mayford, M. (2007). Localization of a stable neural correlate of associative memory. *Science*, *317*, 1230–1233.

Restivo, L., Niibori, Y., Mercaldo, V., Josselyn, S. A., & Frankland, P. W. (2015). Development of adult-generated cell connectivity with excitatory and inhibitory cell populations in the hippocampus. *Journal of Neuroscience*, *35*, 10600–10612.

Rolls, E. (2013). The mechanisms for pattern completion and pattern separation in the hippocampus. *Frontiers in Systems Neuroscience*, *7*, 74.

Sahay, A., Scobie, K. N., Hill, A. S., O'Carroll, C. M., Kheirbek, M. A., Burghardt, N. S., Fenton, A. A., Dranovsky, A., & Hen, R. (2011). Increasing adult hippocampal neurogenesis is sufficient to improve pattern separation. *Nature*, *472*, 466–470.

Snyder, J. S., Clifford, M. A., Jeurling, S. I., & Cameron, H. A. (2012). Complementary activation of hippocampal-cortical subregions and immature neurons following chronic training in single and multiple context versions of the water maze. *Behavioural Brain Research*, *227*, 330–339.

Stone, S. S. D., Teixeira, C. M., DeVito, L. M., Zaslavsky, K., Josselyn, S. A., Lozano, A. M., & Frankland, P. W. (2011). Stimulation of Entorhinal cortex promotes adult neurogenesis and facilitates spatial memory. *The Journal of Neuroscience*, *31*, 13469–13484.

Sun, Q., Sotayo, A., Cazzulino, A. S., Snyder, A. M., Denny, C. A., & Siegelbaum, S. A. (2017). Proximodistal heterogeneity of hippocampal CA3 pyramidal neuron intrinsic properties, connectivity, and reactivation during memory recall. *Neuron*, *95*, 656–672.

Temprana, S. G., Mongiat, L. A., Yang, S. M., Trinchero, M. F., Alvarez, D. D., Kropff, E., Giacomini, D., Beltramone, N., Lanuza, G. M., & Schinder, A. F. (2015). Delayed coupling to feedback inhibition during a critical period for the integration of adult-born granule cells.. *Neuron*, *85*, 116–130.

Teyler, T. J., & DiScenna, P. (1986). The hippocampal memory indexing theory. *Behavioral Neuroscience*, *100*, 147–154.

Thompson, C. L., Pathak, S. D., Jeromin, A., Ng, L. L., MacPherson, C. R., Mortrud, M. T., Cusick, A., Riley, Z. L., Sunkin, S. M., Bernard, A., et al. (2008). Genomic anatomy of the hippocampus. *Neuron*, *60*, 1010–1021.

Tonegawa, S., Pignatelli, M., Roy, D. S., & Ryan, T. J. (2015). Memory engram storage and retrieval. *Current Opinion in Neurobiology*, *35*, 101–109.

Wang, W., Pan, Y.-W., Zou, J., Li, T., Abel, G. M., Palmiter, R. D., Storm, D. R., & Xia, Z. (2014). Genetic activation of ERK5 MAP kinase enhances adult neurogenesis and extends hippocampus-dependent long-term memory. *The Journal of Neuroscience*, *34*, 2130–2147.

Wiskott, L., Rasch, M. J., & Kempermann, G. (2006). A functional hypothesis for adult hippocampal neurogenesis: Avoidance of catastrophic interference in the dentate gyrus. *Hippocampus*, *16*, 329–343.

Witter, M. P. (2007). Intrinsic and extrinsic wiring of CA3: Indications for connectional heterogeneity. *Learning & Memory*, *14*, 705–713.

SUPPORTING INFORMATION

Additional supporting information may be found online in the Supporting Information section at the end of this article.

How to cite this article: Berdugo-Vega, G., Lee, C.-C., Garthe, A., Kempermann, G., & Calegari, F. (2021). Adult-born neurons promote cognitive flexibility by improving memory precision and indexing. *Hippocampus*, *31*(10), 1068–1079. https://doi.org/10.1002/hipo.23373